THE JOURNAL OF BIOLOGICAL CHEMISTRY VOL. 284, NO. 21, pp. 14628–14636, May 22, 2009

Inhibitory Mechanism of *Escherichia coli* RelE-RelB Toxin-Antitoxin Module Involves a Helix Displacement Near an mRNA Interferase Active Site*[S]

Received for publication, December 23, 2008, and in revised form, March 9, 2009 Published, JBC Papers in Press, March 18, 2009, DOI 10.1074/jbc.M809656200

Guang-Yao Li[‡], Yonglong Zhang[§], Masayori Inouye[§], and Mitsuhiko Ikura[‡1]

From the [‡]Division of Signaling Biology, Ontario Cancer Institute, and Department of Medical Biophysics, University of Toronto, Toronto, Ontario M5G 1L7, Canada and the [§]Department of Biochemistry, Robert Wood Johnson Medical School, Piscataway, New Jersey 08854-5635

In *Escherichia coli*, RelE toxin participates in growth arrest and cell death by inducing mRNA degradation at the ribosomal A-site under stress conditions. The NMR structures of a mutant of *E. coli* RelE toxin, $RelE^{R81A/R83A}$, with reduced toxicity and its complex with an inhibitory peptide from RelB antitoxin, $RelB_C$ (Lys^{47}–Leu^{79}), have been determined. In the free $RelE^{R81A/R83A}$ structure, helix α4 at the C terminus adopts a closed conformation contacting with the β-sheet core and adjacent loops. In the $RelE^{R81A/R83A}$-$RelB_C$ complex, helix α3* of $RelB_C$ displaces α4 of $RelE^{R81A/R83A}$ from the binding site on the β-sheet core. This helix replacement results in neutralization of a conserved positively charged cluster of RelE by acidic residues from α3* of RelB. The released helix α4 becomes unfolded, adopting an open conformation with increased mobility. The displacement of α4 disrupts the geometry of critical residues, including Arg^{81} and Tyr^{87}, in a putative active site of RelE toxin. Our structures indicate that RelB counteracts the toxic activity of RelE by displacing α4 helix from the catalytically competent position found in the free RelE structure.

Toxin-antitoxin (TA)[2] systems originally known as suicide or addiction modules, controlling plasmid inheritance through "post-segregational killing" (1, 2), have been documented as an environmental adaptation used by most bacteria (3). Overexpression of certain toxins induces cellular dormancy, also called a quasi-dormant state, which enables cell survival for prolonged times during environmental stresses (4, 5). Recently, TA systems have been linked to medically important phenomena such as biofilm formation and antibiotic resistance (6).

To date, TA toxins are known to perturb one or more vital processes, such as DNA replication, RNA transcription, and protein translation, by targeting DNA gyrase (7), messenger RNA (8, 9), and/or ribosomes (5, 10). A subgroup of toxins, including MazF, RelE, and YoeB, is named as mRNA interferase (11), because they perturb the stability of mRNA by sequence-specific cleavage. Among these toxins, MazF is well established as an ACA sequence-specific endoribonuclease, which cleaves free single-stranded mRNA in the absence of ribosome (12). In contrast, RelE cannot cleave free mRNA transcripts. It cleaves translating mRNA associated with the ribosome at the ribosomal A-site (10). In this manner, RelE is a ribosome-dependent mRNA interferase, and preferential cleavage occurs at the second position of stop codons (UAG, UAA, and UGA) and some sense codons (CAG and UCG), with the UAG (amber) stop codon and the CAG (glutamine) codon being cleaved most efficiently (13). YoeB was initially recognized as a purine-specific endoribonuclease with preference to AG-rich regions, albeit with low efficiency (14). However, it was recently found that YoeB binds to the 50 S subunit in 70 S ribosomes and leads to efficient mRNA cleavage at the ribosomal A-site (15). Therefore, both RelE and YoeB toxins trigger mRNA cleavage in a ribosome-dependent mode, which is distinct from the ribosome-independent mechanism of MazF.

Even though the functionality of *Escherichia coli* RelE has been extensively characterized, the structural mechanism is still elusive. Here we determined the NMR structures of a low toxicity mutant of RelE, $RelE^{R81A/R83A}$, and its complex with the C-terminal region of RelB, $RelB_C$ (Lys^{47}–Leu^{79}). Comparison of the free and $RelB_C$-bound $RelE^{R81A/R83A}$ reveals a large conformational change at the putative active site of the RelE toxin. The present structural studies indicate a direct inhibition mechanism for the RelE-RelB addiction module.

EXPERIMENTAL PROCEDURES

Protein Sample Preparation—Recombinant expression and purification were carried out as described previously for $RelB_C$ (Lys^{47}–Leu^{79}) and wild-type RelE (16). $RelE^{R81A/R83A}$ mutant was obtained using QuikChange site-directed mutagenesis kit (Stratagene). Unlabeled or isotope-enriched (*e.g.* ^{15}N or ^{15}N,^{13}C) protein was purified from crude lysate using nickel-nitrilotriacetic acid resin (Qiagen) and further purified by size exclusion chromatography. For NMR spectroscopy, all samples were prepared in 25 mM sodium phosphate (pH 6.5) containing

* This work was supported, in whole or in part, by National Institutes of Health Grant RO1GM081567 (to M. Inouye). This work was also supported by a grant from Canadian Institutes of Health Research (to M. Ikura) and a Canadian Institutes of Health Research operating grant.

The atomic coordinates and structure factors (codes 2KC8 and 2KC9) have been deposited in the Protein Data Bank, Research Collaboratory for Structural Bioinformatics, Rutgers University, New Brunswick, NJ (http://www.rcsb.org/).

[S] The on-line version of this article (available at http://www.jbc.org) contains supplemental Table 1 and Figs. S1–S6.

[1] Holds the Canada Research Chair in Cancer Structural Biology. To whom correspondence should be addressed: MaRS Toronto Medical Discovery Tower, Rm. 4-804, 101 College St., Toronto, Ontario M5G 1L7, Canada. Tel.: 416-581-7550; Fax: 416-581-7564; E-mail: mikura@uhnres.utoronto.ca.

[2] The abbreviations used are: TA, toxin-antitoxin; NOE, nuclear Overhauser effect; HSQC, heteronuclear single quantum coherence; hetNOE, heteronuclear NOE; r.m.s.d., room mean square deviation.

500 mM NaCl and 1 mM dithiothreitol in 90% H_2O, 10% D_2O, or in 99% D_2O.

Protein Synthesis Inhibition Assay on a Prokaryotic Cell-free System—Prokaryotic cell-free protein synthesis was carried out with an *E. coli* T7 S30 extract system (Promega). The reaction mixture consisted of 10 μl of S30 premix, 7.5 μl of S30 extract, and 2.5 μl of an amino acid mixture (1 mM each of all amino acids except methionine), 1 μl of [^{35}S]methionine, and different amounts of RelE in a final volume of 29 μl. The different amounts of RelE and $RelB_C$ were preincubated for 10 min at 25 °C before the assay started by adding 1 μl of pET-11a-MazG plasmid-DNA (0.16 μg/μl). The reaction was performed for 1.5 h at 37 °C, and proteins were then precipitated with acetone and analyzed by SDS-PAGE followed by autoradiography.

Preparation of E. coli 70 S Ribosomes—70 S ribosomes were prepared from *E. coli* MRE 600 as described previously (17) with minor modifications. Bacterial cells (2 g) were suspended in buffer A (10 mM Tris-HCl (pH 7.8) containing 10 mM $MgCl_2$, 60 mM NH_4Cl, and 6 mM 2-mercaptoethanol). The cells were lysed by French press. After incubation with RNase-free DNase (30 min at 0 °C), cell debris was removed by centrifugation two times at 30,000 rpm for 30 min at 4 °C with a Beckman 50Ti rotor. The supernatant (three-fourth volume from the top) was then layered over an equal volume of 1.1 M sucrose in buffer B (buffer A containing 0.5 M NH_4Cl) and centrifuged at 45,000 rpm for 15 h at 4 °C with a Beckman 50Ti rotor. After washing with buffer A, the ribosome pellets were resuspended in buffer A and applied to a linear 5–40% (w/v) sucrose gradient prepared in buffer A and centrifuged at 35,000 rpm for 3 h at 4 °C with a Beckman SW41Ti rotor. Gradients were fractionated, and the 70 S ribosome fractions were pooled and pelleted at 45,000 rpm for 20 h at 4 °C with a Beckman 50Ti rotor. The 70 S ribosome pellets were resuspended in buffer A before they were stored at −80 °C.

Toeprinting Assays—Toeprinting was carried out as described previously (18) with a minor modification. The mixture for primer-template annealing containing mRNA and ^{32}P-end-labeled DNA primer was incubated at 70 °C for 5 min and then cooled slowly to room temperature. The ribosome-binding mixture contained 2 μl of 10× buffer (100 mM Tris-HCl (pH 7.8) containing 100 mM $MgCl_2$, 600 mM NH_4Cl, and 60 mM 2-mercaptoethanol), different amounts of RelE, 0.375 mM dNTP, 0.05 μM 70 S ribosomal subunits, 1 μM $tRNA_f^{Met}$, and 2 μl of the annealing mixture in a final volume of 20 μl. The final mRNA concentration was 0.035 μM. This ribosome-binding mixture was incubated at 37 °C for 10 min, and then reverse transcriptase (2 units) was added. The cDNA synthesis was carried out at 37 °C for 15 min. The reaction was stopped by adding 12 μl of the sequencing loading buffer (95% formamide, 20 mM EDTA, 0.05% bromphenol blue, and 0.05% xylene cyanol EF). The sample was incubated at 90 °C for 5 min prior to electrophoresis on a 6% polyacrylamide sequencing gel. The *ompA* mRNA was synthesized *in vitro* from a DNA fragment containing a T7 promoter and a part of the opening reading frame using T7 RNA polymerase. The DNA fragment for *ompA* (248 bp), which had the initiation codon at the center, was amplified by PCR using appropriate primers and chromosome DNA as the template. The 5′-end primers for *ompA* contained the T7 promoter sequence.

Nuclear Magnetic Resonance Spectroscopy—NMR spectra were recorded on Inova 500 MHz (Varian) and Avance 600 and 800 MHz (Bruker) spectrometers. All data were collected at 23.5 °C. Backbone and side chain resonance assignments for both free and bound states of $RelB_C$ and $RelE^{R81A/R83A}$ were accomplished with the standard triple resonance experiments described previously (19) (*i.e.* HNCACB, CBCACONH, CCCTOCSYNH, HCCTOCSYNH, and HNCO with samples in 90% H_2O; HCCHCOSY and HCCHTOCSY with samples in 99% D_2O). Both ^{15}N- and ^{13}C-edited nuclear Overhauser effect spectroscopy-HSQC spectra were acquired on ^{15}N,^{13}C-$RelE^{R81A/R83A}$, ^{15}N,^{13}C-$RelE^{R81A/R83A}$-$RelB_C$ and ^{15}N,^{13}C-$RelB_C$-$RelE^{R81A/R83A}$ samples for the final structural calculations. The intermolecular nuclear Overhauser effects (NOE) were distinguished from the intramolecular NOEs by ^{13}C/^{15}N-filtered (F1) ^{13}C-edited (F2) nuclear Overhauser effect spectroscopy-HSQC spectra (20). Compound chemical shift changes of both $RelE^{R81A/R83A}$ and $RelB_C$ upon their interactions were calculated from the chemical shift of H_N, N, CA, and CB nuclei with the weighted formula as described previously (21). All data were processed by using NMRPIPE (22) and analyzed with XEASY (23) and NMRVIEW (24) software packages. Chemical shift data have been deposited in the Biological Magnetic Resonance Bank with accession codes 16065, 16066, and 16067 for the $RelE^{R81A/R83A}$-$RelB_C$ complex, free $RelE^{R81A/R83A}$, and free $RelB_C$, respectively.

Structure Calculation and Refinement—The three-dimensional structures of free $RelE^{R81A/R83A}$ and the $RelE^{R81A/R83A}$-$RelB_C$ complex were calculated using CYANA (25) with standard protocols. NOE-based distance constraints were obtained from a combination of manual and CYANA-based automated NOE assignment procedures (26). Dihedral angle (ϕ/ψ) constraints were estimated from chemical shifts using TALOS (27). Hydrogen bond constraints were generated based on the locations of predicted secondary structure for the protected NH groups in H_2O/D_2O solvent exchange experiments. The final structures were refined using CNS with water as the explicit solvent (28). The atomic coordinates and structure factors have been deposited in the Protein Data Bank with accession codes 2KC8 and 2KC9 for the $RelE^{R81A/R83A}$-$RelB_C$ complex and free $RelE^{R81A/R83A}$, respectively.

RESULTS

$RelB_C$ Abolishes the Residual Catalytic Activity of $RelE^{R81A/R83A}$—Overexpression of wild-type RelE alone in *E. coli* markedly hindered cell growth because of its cytotoxicity. RelB antitoxin neutralizes RelE toxicity by forming a nontoxic complex. Therefore, RelE can be coexpressed with RelB and isolated from the RelB-RelE complex through a denaturation and refolding procedure (16, 29). However, the refolded RelE protein is unstable in solution at elevated concentrations (*i.e.* 0.1–0.2 mM). The resonance assignments of refolded wild-type RelE were hampered by a low signal-to-noise ratio and poor magnetization transfer in three-dimensional NMR experiments. We overcame this obstacle by using a low toxicity

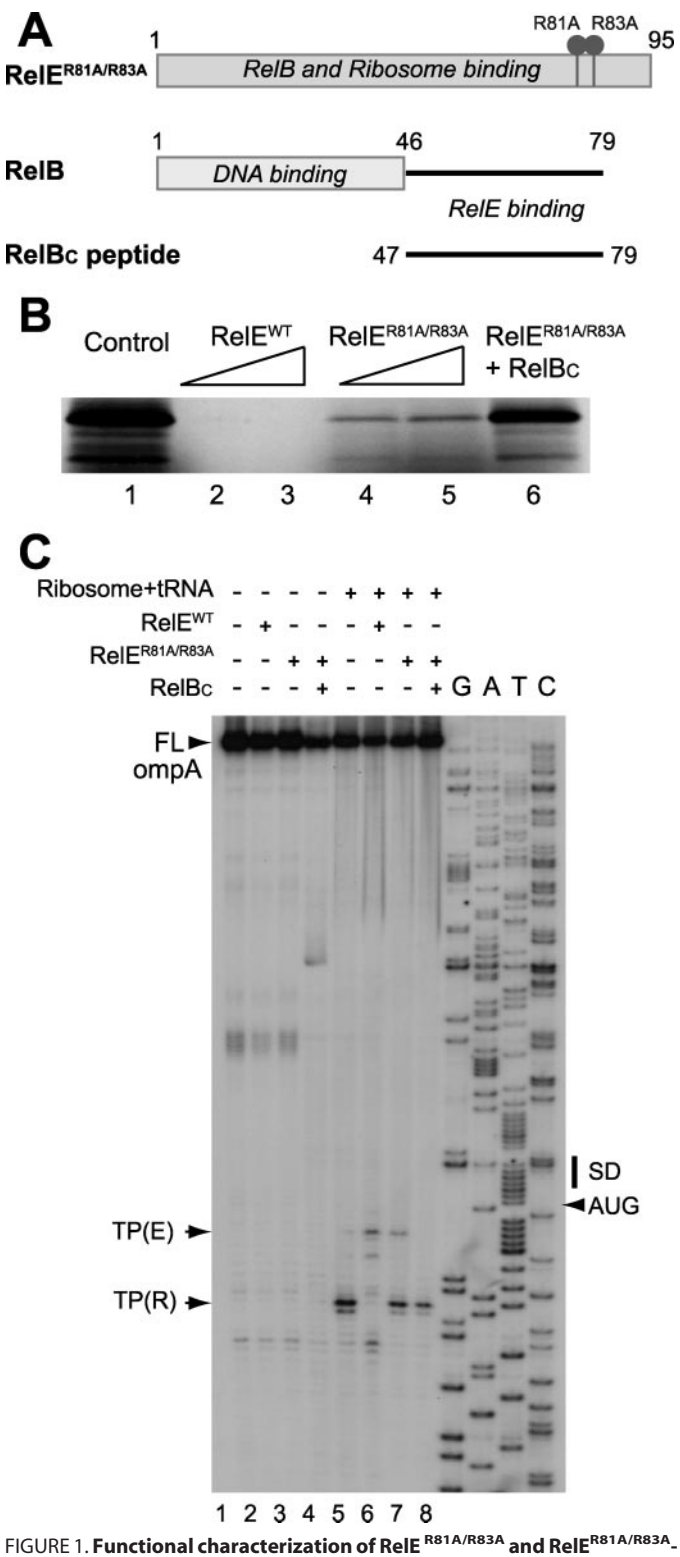

FIGURE 1. **Functional characterization of RelE $^{R81A/R83A}$ and RelE$^{R81A/R83A}$-RelB$_C$.** *A,* domain architects of RelE and RelB. The constructs of RelB$_C$ and RelE$^{R81A/R83A}$ were used in this structural study. *B,* analysis of translation inhibition activity for wild-type RelE, RelE$^{R81A/R83A}$, and RelE$^{R81A/R83A}$-RelB$_C$ complex on MazG synthesis in a prokaryotic cell-free protein synthesis. The control experiment without protein (*lane 1*) and inhibition experiments with 0.15 μg/μl (*lane 2*) and 0.35 μg/μl (*lane 3*) wild type RelE, respectively, are shown; and 0.15 μg/μl (*lane 4*) and 0.35 μg/μl RelE$^{R81A/R83A}$ (*lane 5*), respectively, and 0.35 μg/μl RelE$^{R81A/R83A}$-RelB$_C$ (*lane 7*) are shown. *C,* analysis of the ribosome-dependent mRNA cleavage activity for RelE, RelE$^{R81A/R83A}$, and RelE$^{R81A/R83A}$-RelB$_C$ complex on *ompA* mRNA in a toeprinting analysis. The *ompA* mRNAs were synthesized *in vitro* from a 248-bp DNA fragment containing a T7 promoter using T7 RNA polymerase. The sequence ladder shown at the *right-hand side* was obtained using the same primer used for toeprinting with pCR®2.1-TOPO®-*ompA* as template. Control experiments are shown without protein and ribosome (*lane 1*), with 0.1125 μg/μl wild-type RelE (*lane 2*), with 0.1125 μg/μl RelE$^{R81A/R83A}$ (*lane 3*), and with 0.1125 μg/μl RelE$^{R81A/R83A}$-RelB$_C$ (*lane 4*). Toeprinting experiments are shown with 0.05 μM 70 S ribosomes and 1 μM tRNA$_f^{Met}$ (*lane 5*), 0.05 μM 70 S ribosomes and 1 μM tRNA$_f^{Met}$ with 0.1125 μg/μl wild-type RelE (*lane 6*), 0.05 μM 70 S ribosomes and 1 μM tRNA$_f^{Met}$ with 0.1125 μg/μl RelE$^{R81A/R83A}$ (*lane 7*), and 0.05 μM 70 S ribosomes and 1 μM tRNA$_f^{Met}$ with 0.1125 μg/μl RelE$^{R81A/R83A}$-RelB$_C$ (*lane 8*). The initiation codon, AUG, is indicated with an *arrow*. The full-length product of primer extension is denoted as *FL*. Positions of ribosome toeprinting and RelE toeprinting bands are indicated as *TP*(*R*) and *TP*(*E*), respectively.

mutant, RelE$^{R81A/R83A}$ (Fig. 1*A*), which allowed us to purify enough protein under native conditions for structural studies.

Comparison of the mRNA interferase activity of wild-type RelE with RelE$^{R81A/R83A}$ indicates that the mutation significantly reduces but does not abolish its activity in both cell-free protein synthesis (Fig. 1*B*) and toeprinting assays (Fig. 1*C*). The residual activity of RelE$^{R81A/R83A}$ is completely abolished by the addition of the C-terminal domain of RelB antitoxin, RelB$_C$ (residues Lys^{47} to Leu^{79}) (Fig. 1, *A*–*C*). These observations suggest that RelE$^{R81A/R83A}$ represents a structural model of wild type in an active conformation, whereas the complex of RelE$^{R81A/R83A}$ and RelB$_C$ represents a model of an inactive conformation.

The structural properties of RelE$^{R81A/R83A}$ mutant and wild-type RelE were compared using NMR spectroscopy. The ^{1}H-^{15}N HSQC spectra of the mutant in both free and RelB$_C$-bound states show high similarity to those of the wild type, indicating the structural integrity and the ability for RelB binding were not significantly affected by the mutagenesis (Fig. 2*A* and supplemental Fig. S1). The affinities of RelB$_C$ binding to wild-type RelE and RelE$^{R81A/R83A}$ mutant were then measured using an intrinsic tryptophan fluorescence method, by the virtue of only one tryptophan residue (Trp^{15}) existing in RelE toxin. The dissociation constant (K_D) of wild type is 154 ± 15 nM and that of RelE$^{R81A/R83A}$ is 200 ± 24 nM, indicating that the mutational effect on the affinity is marginal (supplemental Fig. S2).

RelE$^{R81A/R83A}$ and RelB$_C$ Interaction Characterized by NMR Spectroscopy—A substantial improvement in line width and magnetization transfer was observed for spectra recorded on RelE$^{R81A/R83A}$ compared with the refolded wild-type RelE (Fig. 2*A* and supplemental Fig. S1). Titration of ^{15}N,^{13}C-labeled RelE$^{R81A/R83A}$ with unlabeled RelB$_C$ showed significant chemical shift perturbation in the ^{1}H-^{15}N HSQC spectrum (Fig. 2, *A* and *C*). A pair of NH resonances corresponding to each residue in both free and RelB$_C$-bound states was observed during the titration, indicative of a slow exchange regime on the NMR time scale. The slow exchange spectral change is consistent with a high affinity in the range of 10^{-7} M. A ^{1}H-^{15}N HSQC spectrum of ^{15}N,^{13}C-labeled RelB$_C$ alone displays poor dispersion of NH resonance (7.9 – 8.5 ppm), indicating that this C-terminal region of RelB is largely unstructured in its free state (Fig. 2*B*). Titration of labeled RelB$_C$ with unlabeled RelE$^{R81A/R83A}$ shows dramatic chemical shift changes in a similar slow exchange regime (Fig. 2, *B* and *D*). The well dispersed spectrum of RelB$_C$ in the bound state suggests that RelE$^{R81A/R83A}$ binding induces the folding of RelB$_C$.

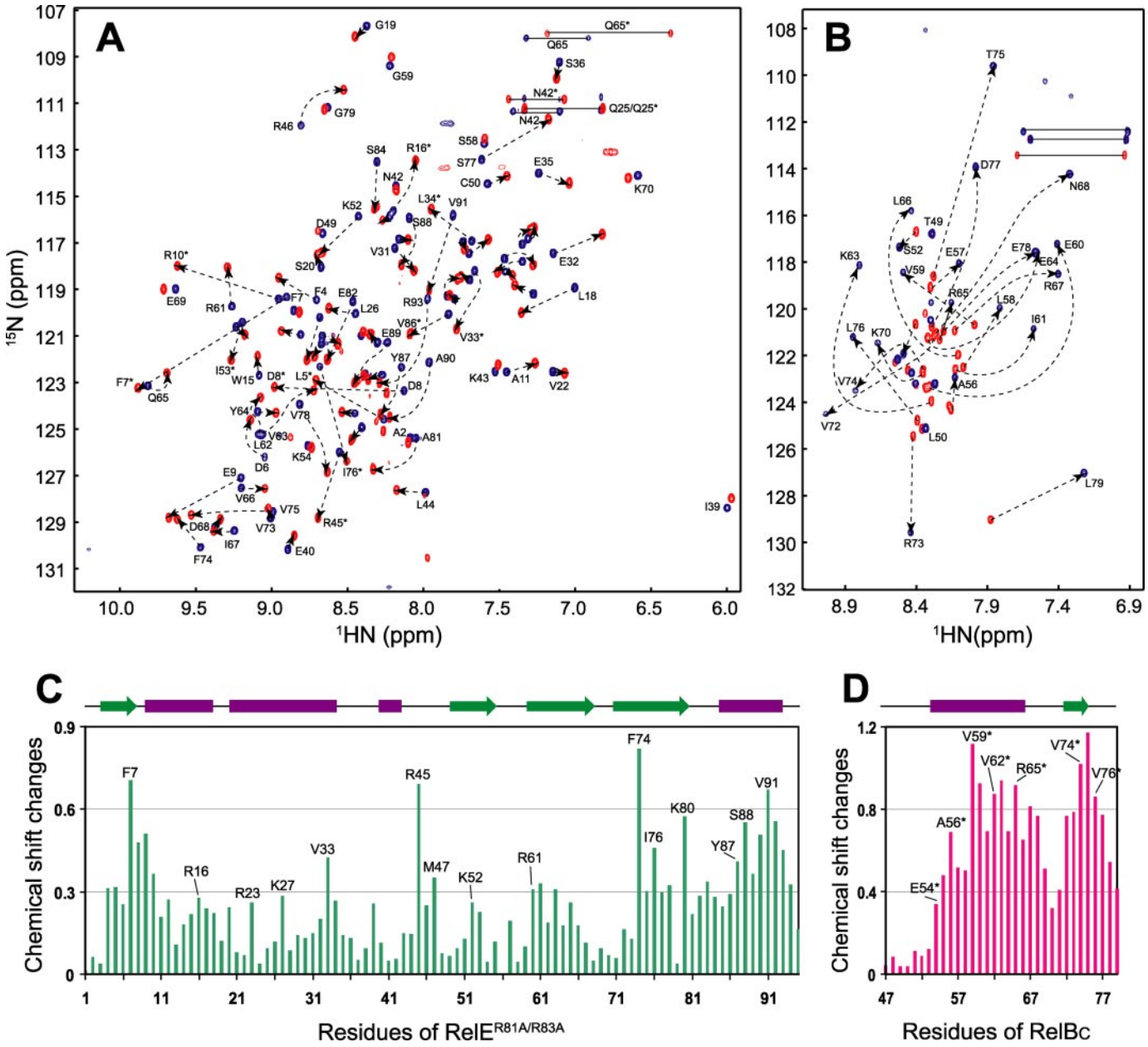

FIGURE 2. **Interaction of RelE$^{R81A/R83A}$ and RelB$_C$ characterized by NMR.** *A*, superimposed ^{1}H-^{15}N HSQC spectra of free (*blue*) and RelB$_C$-bound (*red*) RelE$^{R81A/R83A}$. *B*, superimposed ^{1}H-^{15}N HSQC spectra of free (*red*) and RelE$^{R81A/R83A}$-bound RelB$_C$ (*blue*). *C*, averaged chemical shift changes of individual residues in RelE$^{R81A/R83A}$ perturbed by RelB$_C$ binding. *D*, averaged chemical shift changes of individual residues in RelB$_C$ upon binding to RelE$^{R81A/R83A}$. The averaged chemical shift changes are calculated by a weighted combination of chemical shifts of H_N, N, CA, and CB nuclei (21).

Resonance assignments of RelE$^{R81A/R83A}$ and RelB$_C$ in both free and bound states were accomplished using a standard set of triple resonance procedures (19). The chemical shift index analysis (30) of RelB$_C$ peptide in both free and bound states revealed a disordered-to-ordered conformation change upon the complex formation (supplemental Fig. S3, *A* and *B*). On the other hand, the chemical shift index analysis of RelE$^{R81A/R83A}$ revealed an unfolding of a C-terminal helix (α4) coupled with RelB$_C$ binding (supplemental Fig. S3, *C* and *D*). The three-dimensional structures of RelE$^{R81A/R83A}$ alone and in complex with RelB$_C$ were determined by using a combination of manual and automated NOE assignment procedures (supplemental Table 1).

Structures of RelE$^{R81A/R83A}$—The ensemble of the 20 lowest energy structures of RelE$^{R81A/R83A}$ shows a well defined α/β sandwich fold with approximate dimensions of 36 × 30 × 30 Å (Fig. 3*A*). The overall topology is $\beta\alpha\alpha\alpha\beta\beta\beta\alpha$, in which four strands form a β-sheet core surrounded by four α-helices (Fig. 3*B*). Three consecutive anti-parallel β-strands (β2–β4) pack into a classic meander motif (31), providing a scaffold for folding of the protein. The N-terminal strand (β1) and the helix hairpin, formed by two long helices (α1 and α2), are tightly associated to one side of the β-meander core through numerous hydrophobic contacts. In particular, the hydrophobic residues (Val^{22}, Leu^{26}, Leu^{30}, Val^{31}, Val^{33}, and Leu^{34}) from the amphipathic α2 form extensive contacts with one side of the

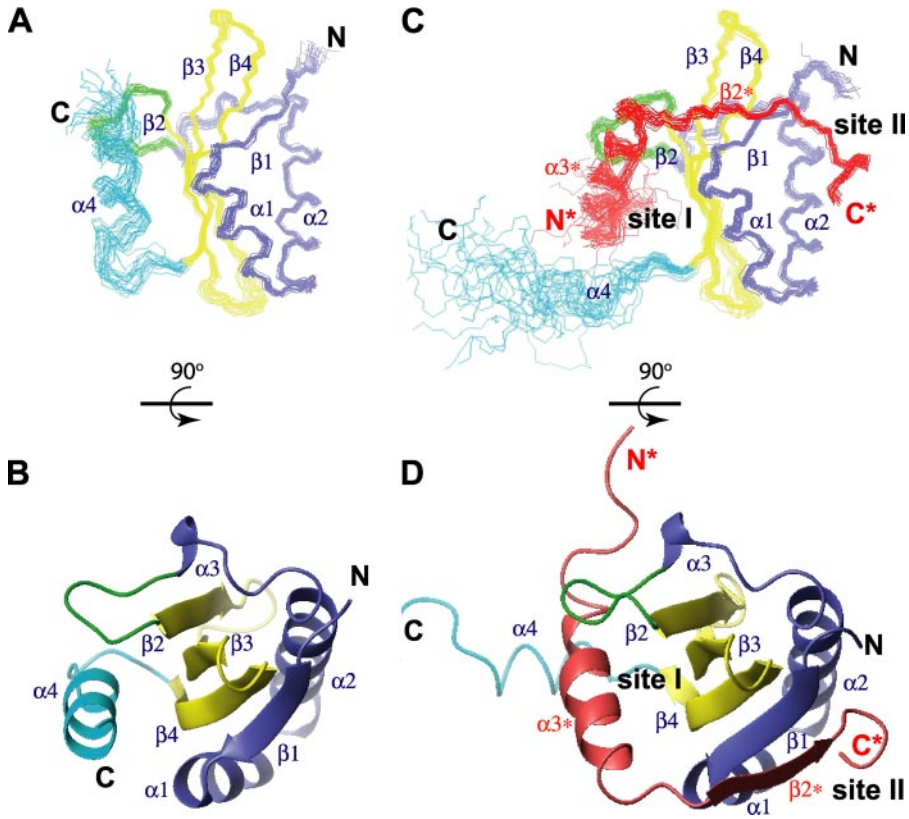

FIGURE 3. **Structures of RelE$^{R81A/R83A}$ and RelE$^{R81A/R83A}$-RelB$_C$.** *A,* ensemble of the 20 lowest energy structures of RelE$^{R81A/R83A}$. *B, ribbon* representation of the lowest energy structure of RelE$^{R81A/R83A}$ rotated 90° showing the β-sheet core surrounded by four helices. *C,* ensemble of the 20 structures of the RelE$^{R81A/R83A}$-RelB$_C$ complex. *D, ribbon* representation showing the helix replacement and formation of the inter-molecular β-sheet. Interface site I and II are indicated in the complex structure. The N-terminal isolated strand β1 and helix hairpin (α1-α2) region of RelE$^{R81A/R83A}$ (Met^1–Asn^{42}) is colored in *blue*, loop α3-β2 in *green*, the central β-meander motif (β2-β4) in *yellow*, and the C-terminal tail (Ala^{81}–Leu^{95}) in *cyan*. The antitoxin RelB$_C$ peptide is colored in *red*.

twisted β-sheet, which is composed entirely of hydrophobic residues (Leu^5 and Phe^7 from β1; Ile^{53} and Leu^{55} from β2; Tyr^{60}, Leu^{62}, Tyr^{64}, and Val^{66} from β3; and, Val^{73}, Val^{75}, and Val^{78} from β4). A long linking region that connects α2 and β2 wraps around the same side of the β-sheet, providing additional stabilizing interactions to the main hydrophobic core. A short 3_{-10} helix (α3) is situated in the middle of the long loop region. In contrast, the other side of the central β-sheet is more exposed to solvent. The C terminus of RelE$^{R81A/R83A}$ forms a helix (α4), which associates with the protruded surface of the central β-meander motif. This interaction is supported by α3-β2 loop and β1-α1 junction regions through both hydrophobic and electrostatic contacts (Fig. 3, *A* and *B* and Fig. 4*A*), burying a total surface area of ~1100 Å^2. A positively charged and highly conserved cluster (including Arg^{45}, Lys^{52}, Lys^{54}, Arg^{56}, Arg^{61}, Lys^{80}, Arg^{81}, and Arg^{83}) is located adjacent to the interface of the β-sheet and helix α4 (Fig. 4*D*). Structural comparison with known RNases and mutagenesis in the previous (10, 29, 32) and present studies suggest that the positively charged cluster represents a putative mRNA substrate-binding site. Residues from both main domains of RelE and the C-terminal α4 helix form an active site for the toxicity of RelE. Hence the closed conformation of α4 is in a catalytically competent position (details under "Discussion").

Structure of RelE$^{R81A/R83A}$-RelB$_C$ Complex—The RelB$_C$ peptide folds into a helix (α3*, Glu^{54*}–Leu^{66*}, number of residues and secondary structure elements refer to full-length RelB, asterisk is used to denote RelB throughout) and a short β-strand (β2*, Val^{72*}–Val^{74*}) upon binding to RelE$^{R81A/R83A}$ (Fig. 3, *C* and *D*). Two prolines (Pro^{69} and Pro^{71}) mediate the formation of a turn between helix α3* and strand β2*, bending the polypeptide chain by ~90°. This perpendicular orientation of α3* and β2* provides a concave surface that interacts with a convex interface on RelE. The α3* contacts with the surface of the central β-meander motif, termed interface site I, and the β2* contacts with the surface formed by β1-α1-α2 elements of RelE, termed interface site II. At site I, helix α3* of RelB$_C$ displaces α4 of RelE$^{R81A/R83A}$, through hydrophobic interactions with β3 (Val^{63}), β4 (Ile^{76}), and loop α3-β2 (Leu^{44} and Met^{47}) (Fig. 4, *A* and *B*). However, the orientation of α3* along the β-sheet surface is tilted by 36° compared with α4. An acidic patch (Asp^{53*}, Glu^{54*}, Asp^{55*}, and Glu^{57*}) at the N terminus of helix α3* of RelB$_C$ (Fig. 4, *B* and *F*) directly neutralizes the positively charged cluster at the putative RNA-binding site of RelE$^{R81A/R83A}$ (Arg^{45}, Lys^{52}, Lys^{54}, and Arg^{61}) (Fig. 4*E*). At site II, the β2* of RelB$_C$ forms an inter-molecular anti-parallel β-sheet with adjacent β1 of RelE$^{R81A/R83A}$. The remaining C-terminal residues of RelB$_C$ form a rigid turn conformation and anchor to the surface of the α1-α2 hairpin (Fig. 4*C*). Hydrophobic side chains of Val^{74*}, Leu^{76*}, and Leu^{79*} from RelB$_C$ interact with a hydrophobic patch of RelE$^{R81A/R83A}$ formed by residues from β1 (Leu^5 and Phe^7), α1 (Leu^{12} and Trp^{15}), and α2 (Leu^{30} and Val^{31}). The unique chemical shifts of δ1 (0.09 ppm) and δ2 (−0.61 ppm) protons of Leu^{79*} are consistent with the determined structure, in which methyl groups of Leu^{79*} point to the center of the hydrophobic pocket and pack against the indole ring of Trp^{15}. Solvent-exposed basic residues (Arg^{16}, Arg^{23}, Lys^{27}, and Lys^{28}) surround the hydrophobic patch, forming another positively charged surface (Fig. 4*H*), which is neutralized by Asp^{77*} and Glu^{78*} and the C-terminal carboxylate group of Leu^{79*} (Fig. 4*I*). Overall, both hydrophobic and electrostatic forces stabilize the complex formation of RelE$^{R81A/R83A}$ and RelB$_C$. In total, RelB$_C$ peptide buries a large solvent-accessible surface area of about 2700 Å^2, which encompasses both site I and site II.

RelB Perturbs the Integrity of the Active Site of RelE by Inducing Conformational Changes—Comparison of RelB$_C$-bound RelE$^{R81A/R83A}$ to the unbound structure reveals a pronounced

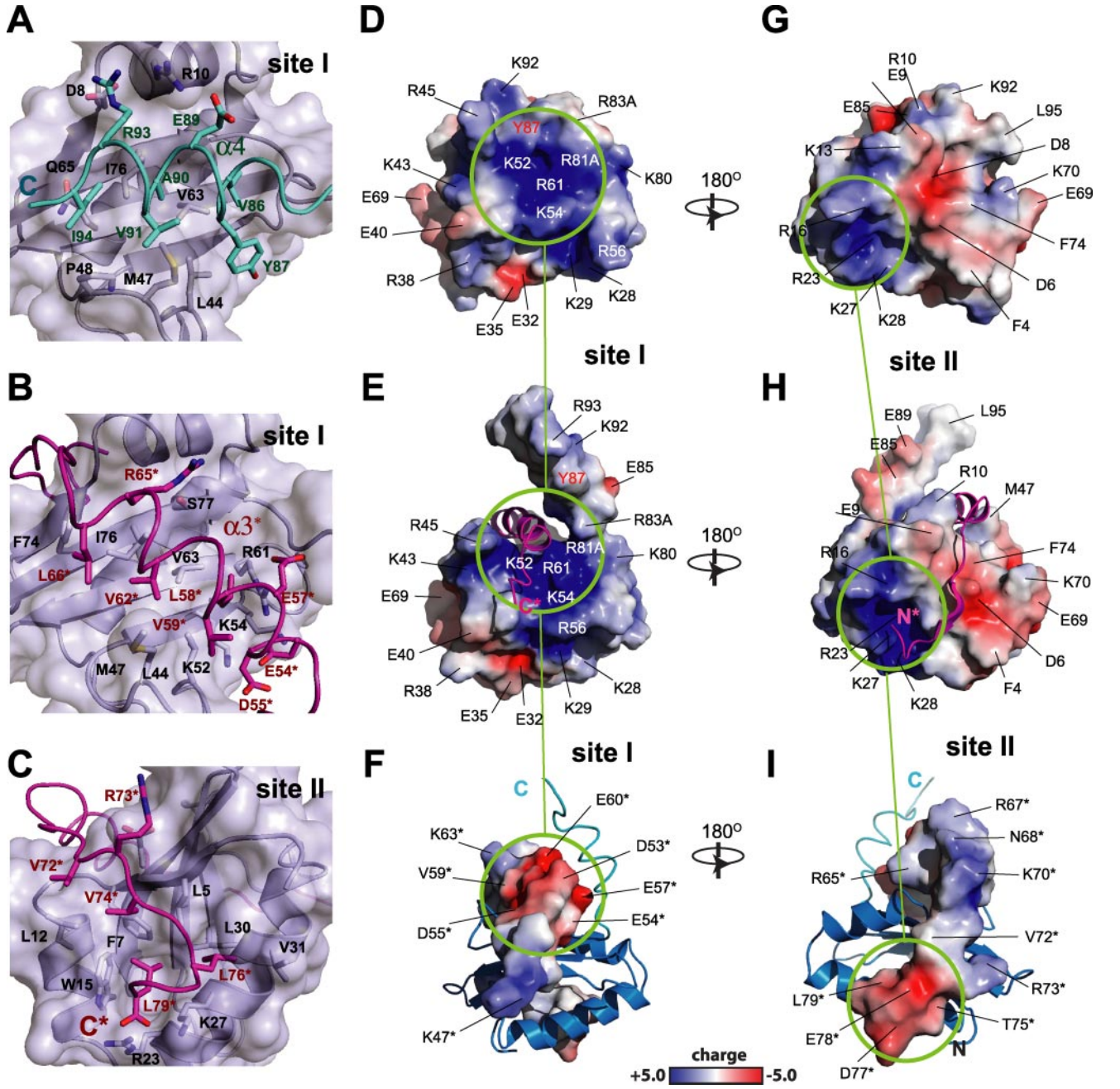

FIGURE 4. **The interface and electrostatic properties of RelE$^{R81A/R83A}$ and RelB$_C$.** *A,* helix α4 occupies the surface of the central β-meander motif and interacts with the α3-β2 loop and β1-α1 junction region. Helix α4 is colored in *cyan*, and the remaining core structure of RelE is colored in *gray*. *B,* interface site I. The helix α3* of RelB (*magenta*) occupies the surface of β-sheet core of RelE (*gray*). *C,* interface site II. The C-terminal extended region of RelB (*magenta*) anchors on the surface of the RelE β1, α1, and α2 (*gray*). The electrostatic surface analysis of free RelE$^{R81A/R83A}$ (*D*), RelB$_C$-bound RelE$^{R81A/R83A}$ (*E*), and RelE$^{R81A/R83A}$-bound RelB$_C$ (*F*). *G–I,* opposite views of *D--F* with a rotation of 180°. Two positively charged clusters on the RelE$^{R81A/R83A}$ surface are complemented by negatively charged clusters from RelB$_C$, which are denoted by *light green circles*. The main positive cluster of the RelE$^{R81A/R83A}$ protein shown in *D–F* is the putative mRNA-binding site.

conformational change of α4 and adjacent loops (loop α3-β2 and β4-α4). The α4 swings out from the surface of the central β-sheet as it is displaced by the amphipathic helix α3* from RelB$_C$ in the complex (Figs. 3 and 4). The large chemical shift perturbation in the C-terminal tail region of RelE$^{R81A/R83A}$ by RelB$_C$ is because of a conformational change rather than direct interaction (Fig. 2, *A* and *C*, and supplemental Fig. S4, *A* and *B*). The released α4 becomes unfolded, as evidenced by the chemical shift index analysis results (supplemental Fig. S3, *C* and *D*).

To further probe the structure and dynamic nature of the RelE toxin, we examined the internal motion of RelE$^{R81A/R83A}$ by measuring ^{1}H-^{15}N heteronuclear NOE (hetNOE) relaxation data (supplemental Fig. S5, *A* and *B*). With the exception of the N- and C-terminal residues, the hetNOE values for the main domain of RelE$^{R81A/R83A}$ in both free and RelB$_C$-bound states are relatively uniform. The relatively high magnitude of the NOE values (>0.8) for residues within the structured core domain (residues 4–79) is characteristic of a well folded glob-

ular structure. By contrast, the C-terminal tail region (residues 80–95) displays lower hetNOE values (0.5–0.7) in the $RelB_C$-free state than that seen for the core domain. These data indicate that the C-terminal helix α4 possesses an increased internal mobility despite the fact that the tail is found as part of the folded structure in the $RelB_C$-free state of $RelE^{R81A/R83A}$. The transverse relaxation rate (R_2) values of residues in this tail region as well as in the adjacent loops are significantly higher than the average value of the whole protein in the free state (supplemental Fig. S5*C*). It is likely that this region undergoes a conformational exchange between the associated (closed) state found in the NMR-driven structure and an isolated (open) state that could not be seen in the structure. Upon binding of $RelB_C$, $RelE^{R81A/R83A}$ displays large changes in both the hetNOE and R_2 values, especially around the C-terminal helix α4 region. A dramatic reduction in hetNOE and R_2 values within the α4 region is observed, indicating an increase in the mobility of this region (supplemental Fig. S5, *B* and *D*). This observation is fully consistent with the release of this helix from the core structure upon $RelB_C$ binding. Concomitant to this structure and dynamic change associated with α4, the dynamic property of the loop α3-β2 region is also significantly altered by $RelB_C$ binding; residues Leu^{44}, Gly^{46}, and Asp^{49} become more dynamic in the bound state than in the free state (supplemental Fig. S5). This region is in close proximity to the C-terminal helix α4 in the free state and the α3* in the bound state, and is presumably affected by the conformational change associated with the toxin-antitoxin interaction.

DISCUSSION

Among the toxin-antitoxin systems, RelE family toxins have the widest phylogenetic distribution in the prokaryotic genomes (8), being found in diverse bacterial and archaeal lineages (33). The *E. coli* RelE is one of the best characterized TA toxins in terms of both *in vivo* and *in vitro* functional studies (13, 29); however, the structure of *E. coli* RelE has never been reported. In the previous studies (13, 29), substitution of the last six residues (AVKRIL) into a VTVTVT amino acid sequence resulted in a nontoxic version of RelE, $RelE_{CS6}$, thereby indicating the C-terminal region is functionally important for the toxicity of RelE. Our structural studies of $RelE^{R81A/R83A}$ revealed a large conformational rearrangement in the C terminus upon interaction with an inhibitory antitoxin peptide $RelB_C$. In the absence of the antitoxin peptide, the last 10 C-terminal residues form an amphipathic helix α4 folded on the surface of the central β-sheet. The α4 residues (Val^{86}, Tyr^{87}, Ala^{90}, and Arg^{94}) involved in the intra-molecular interaction with the core domain (Fig. 4*A*) are highly conserved within the RelE family of toxins (8), indicating that the position of the C-terminal helix in a closed conformation may be a common feature in the family of proteins.

In a structural similarity search using DALI (34), YoeB toxin (14) from *E. coli* (Z score = 10, r.m.s.d. = 1.9 Å) and archaeal RelE (32) (called aRelE) from *Pyrococcus horikoshii* (Z score = 10, r.m.s.d. = 2.5 Å) were identified as the best matches with the present structure of *E. coli* RelE. Among these structures, the helix hairpin and the β-meander motif are conserved. However, there are several distinct differences between them (supplemental Fig. S6). First, the elongated C-terminal extension of α4 in *E. coli* RelE is not present in aRelE and YoeB toxins. Second, there is a short strand inserted at the N-terminal side of the conserved three-strand β-meander motif in both aRelE and YoeB; however, this insertion is too short to form a secondary structural element in the structure of *E. coli* RelE. Instead, it forms a relatively rigid loop α3-β2 (Fig. 3, *B* and *D*). In addition, the lengths of α1 and the strands in the central β-meander motif differ in YoeB and RelE/aRelE. The α1 is much shorter in RelE and aRelE (8 residues) than in YoeB (17 residues), whereas the meander strands are longer in RelE and aRelE than in YoeB (supplemental Fig. S6). RelE also shows structural similarities, with low Z scores and small r.m.s.d. values, to other microbial ribonucleases such as the C-terminal ribonuclease domain of colicin-Glu[5] (35), a tRNase from *E. coli* (Z score = 3.7, r.m.s.d. = 3.0 Å) and RNase SA (36), a guanyl-specific ribonuclease from *Streptomyces aureofaciens* (Z score = 3.2, r.m.s.d. = 3.0 Å). The structural architecture consisting of a two-layer α/β sandwich and an RNA recognition site on the surface of the central β-sheet are highly conserved among these RNA-binding proteins (supplemental Fig. S6).

Comparison of RelE with the well characterized RNase SA revealed that RNA substrate-binding residues are conserved in the two proteins (36). In *E. coli* RelE, Leu^{44} and Tyr^{87} are proposed to provide a site for base packing, and Arg^{61} is proposed to promote backbone phosphate recognition (Fig. 5*A*). In contrast, residues compared with the canonical catalytic triad of RNase SA are not present in RelE. The catalytic His^{85} and Glu^{54} of RNase SA (Fig. 5*B*) and His^{83} and Glu^{46} of YoeB (14) (Fig. 5*C*) are replaced with Arg^{81} and Lys^{52} in *E. coli* RelE, respectively (Fig. 5*A*). Despite the nonconservation, RelE and YoeB toxins share the similar microbial RNase fold. The lack of catalytic residues in RelE renders RelE alone nonfunctional in cleaving free mRNA by itself. The enzymatic activity is only achieved upon association with the ribosome. Although YoeB shows weak intrinsic endoribonuclease activity, our recent data (15) demonstrate that YoeB is a potent protein synthesis inhibitor by cleaving mRNA at the ribosomal A-site. It is intriguing to propose that RelE and YoeB toxins share similarity in their mRNA interferase activity in the ribosome-dependent mode, which is distinct from the mechanisms of the canonical microbial RNases and the ribosome-independent mRNA interferase MazF.

Structural comparison of RelE in free (active) and antitoxin-bound (inactive) states revealed a large conformational change induced by RelB binding. In the active state of RelE, the conserved Tyr^{87} in α4 is in close proximity with Arg^{81} in the β4-α4 loop and Leu^{44} in the α3-β2 loop (Fig. 5*A*). This side chain arrangement, apparently required for the cleavage of mRNA at the ribosomal A-site, resembles the active site structure of RNase SA, supporting the hypothesis that this site is an active site of RelE. In the inactive state of RelE complexed with RelB, Tyr^{87} moves away from Arg^{81} and Leu^{44}, as α4 is released from the core domain by the binding of RelB. This situation rather resembles the orientation of corresponding side chains found in the crystal structure of the archaean aRelE-aRelB complex (32), known to be an inactive conformation. These results are consistent with the previous study of inactive $RelE_{CS6}$ (13), in

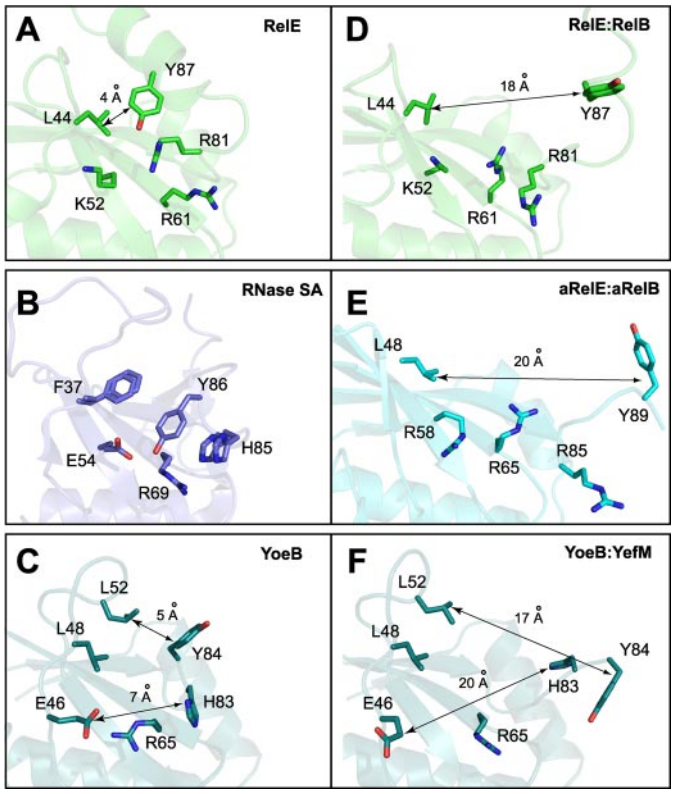

FIGURE 5. **RelB induced conformation change in the active site of RelE.** *A,* active conformation of the *E. coli* RelE mRNA-binding site in the absence of RelB antitoxin. The side chain of Arg^{81} was modeled based on the orientation of Ala^{81} in the structure of $RelE^{R81A/R83A}$. *B,* active site of RNase SA shows the catalytic triad (Glu^{54}, Arg^{69}, and His^{85}) and the hydrophobic site (Phe^{37} and Tyr^{86}) for base packing. *C,* catalytic site of YoeB in the YefM-free conformation shows the catalytic triad (Glu^{46}, Arg^{65}, and His^{83}) and base anchor residues (Leu^{48}, Leu^{52}, and Tyr^{84}). *D,* putative mRNA-binding site of *E. coli* RelE in the presence of $RelB_C$ shows a large conformation disruption to the active site. The side chain of Arg^{81} is modeled based on the orientation of Ala^{81} in the structure of $RelE^{R81A/R83A}$-$RelB_C$. *E,* active site of archaeal aRelE in the aRelB-aRelE complex shows an inactive conformation similar to the $RelE^{R81A/R83A}$-$RelB_C$ complex. The C-terminal residues (Tyr^{89} and Lys^{90}) of aRelE are missing in the crystal structure; they were arbitrarily rebuilt to estimate the position of Tyr^{89}. *F,* catalytic active site of YoeB in the YoeB-YefM complex shows the conformational change altered by YefM binding.

which the substitution of the C-terminal six residues alters the conformation of $\alpha 4$ by disrupting the interaction between the C-terminal tail and the core domain. A similar conformational rearrangement in the active site is seen in the YoeB-YefM TA system (14), which also involves a large movement of residues in the C terminus of the protein (His^{83} and Tyr^{84} in Fig. 5, *C* and *F*), although YoeB toxin has a much shorter C-terminal tail. The perturbation of the proper arrangement of critical residues at an active site seems to be a common theme for the inactivation mechanism of RelE/ParE superfamily TA systems.

At present, the positioning of the catalytically active RelE in the ribosome is unknown. However, mRNA cleavage by RelE requires a vacant A-site and substrate mRNA anchored on the 30 S subunit, suggesting that RelE binds in a region that overlaps with the "decoding center" within the ribosomal A-site (13). It is known that the ribosome is a catalytically active ribozyme that can cleave mRNA even in the absence of RelE. RelE may modulate its substrate specificity by altering the conformation of the ribosome and/or the associated mRNA at the A-site decoding region. It is most likely that RelE functions as a stimulatory factor, which stabilizes the catalytically active conformation of ribosomal RNA. However, in view of the fact that RelE has the side chain arrangement similar to that of RNase SA (36), it is highly possible that a complete catalytic active center may be formed only when RelE and ribosome associate to a holoenzyme.

Although the molecular detail of mRNA and ribosome binding remains to be addressed by further structural studies, previous studies using site-directed mutagenesis in *P. horikoshii* aRelE (32) and *E. coli* RelE toxins (29) illuminated that the arginine (Arg^{85} in aRelE and Arg^{81} in RelE) at the conserved histidine position in canonical RNases is crucial for the function of RelE toxins. This residue could play a role in the ribosome recognition or be involved in the formation of a catalytic center together with ribosome. Our structural studies provide evidence that RelB antitoxin directly inhibits RelE toxin through binding to the active site, although the formation of a $RelE_2$-$RelB_2$ complex mediated through the N-terminal dimerization domain of RelB (16) may also spatially block RelE from entering the ribosomal A-site where the RNA cleavage takes place, a mechanism proposed by Takagi *et al.* (32). Nevertheless, further studies are required to elucidate exactly how RelE collaborates with the ribosome for enzymatic activity.

Acknowledgments—We thank Christopher B. Marshall, Peter B. Stathopulos, and Emma Gooding for critical reading of the manuscript. CFI funding was received for Bruker 600 and Bruker 800 MHz NMR spectrometers.

REFERENCES

1. Gerdes, K., Jacobsen, J. S., and Franch, T. (1997) *Genet. Eng.* **19,** 49–61
2. Engelberg-Kulka, H., and Glaser, G. (1999) *Annu. Rev. Microbiol.* **53,** 43–70
3. Gerdes, K., Christensen, S. K., and Lobner-Olesen, A. (2005) *Nat. Rev. Microbiol.* **3,** 371–382
4. Suzuki, M., Zhang, J., Liu, M., Woychik, N. A., and Inouye, M. (2005) *Mol. Cell* **18,** 253–261
5. Liu, M., Zhang, Y., Inouye, M., and Woychik, N. A. (2008) *Proc. Natl. Acad. Sci. U. S. A.* **105,** 5885–5890
6. Lewis, K. (2008) *Curr. Top. Microbiol. Immunol.* **322,** 107–131
7. Bahassi, E. M., O'Dea, M. H., Allali, N., Messens, J., Gellert, M., and Couturier, M. (1999) *J. Biol. Chem.* **274,** 10936–10944
8. Anantharaman, V., and Aravind, L. (2003) *Genome Biol.* **4,** R81
9. Condon, C. (2006) *Mol. Microbiol.* **61,** 573–583
10. Christensen, S. K., and Gerdes, K. (2003) *Mol. Microbiol.* **48,** 1389–1400
11. Yanaguchi, Y., and Inouye, M. (2009) *Prog. Mol. Biol. Transl. Sci.* **85,** 467–500
12. Zhang, Y., Zhang, J., Hoeflich, K. P., Ikura, M., Qing, G., and Inouye, M. (2003) *Mol. Cell* **12,** 913–923
13. Pedersen, K., Zavialov, A. V., Pavlov, M. Y., Elf, J., Gerdes, K., and Ehrenberg, M. (2003) *Cell* **112,** 131–140
14. Kamada, K., and Hanaoka, F. (2005) *Mol. Cell* **19,** 497–509
15. Zhang, Y., and Inouye, M. (2009) *J. Biol. Chem.* **284,** 6627–6638
16. Li, G. Y., Zhang, Y., Inouye, M., and Ikura, M. (2008) *J. Mol. Biol.* **380,** 107–119
17. Aoki, H., Ke, L., Poppe, S. M., Poel, T. J., Weaver, E. A., Gadwood, R. C., Thomas, R. C., Shinabarger, D. L., and Ganoza, M. C. (2002) *Antimicrob. Agents Chemother.* **46,** 1080–1085
18. Moll, I., and Blasi, U. (2002) *Biochem. Biophys. Res. Commun.* **297,** 1021–1026
19. Kanelis, V., Forman-Kay, J. D., and Kay, L. E. (2001) *IUBMB Life* **52,** 291–302

20. Zwahlen, C., Legault, P., Vincent, S. J. F., Greenblatt, J., Konrat, R., and Kay, L. E. (1997) *J. Am. Chem. Soc.* **119,** 6711–6721
21. Mal, T. K., Masutomi, Y., Zheng, L., Nakata, Y., Ohta, H., Nakatani, Y., Kokubo, T., and Ikura, M. (2004) *J. Mol. Biol.* **339,** 681–693
22. Delaglio, F., Grzesiek, S., Vuister, G. W., Zhu, G., Pfeifer, J., and Bax, A. (1995) *J. Biomol. NMR* **6,** 277–293
23. Bartels, C., Xia, T., Billeter, M., Guntert, P., and Wuthrich, K. (1995) *J. Biomol. NMR* **6,** 1–10
24. Johnson, B. A. (2004) *Methods Mol. Biol.* **278,** 313–352
25. Guntert, P., Mumenthaler, C., and Wuthrich, K. (1997) *J. Mol. Biol.* **273,** 283–298
26. Herrmann, T., Guntert, P., and Wuthrich, K. (2002) *J. Mol. Biol.* **319,** 209–227
27. Cornilescu, G., Delaglio, F., and Bax, A. (1999) *J. Biomol. NMR* **13,** 289–302
28. Brunger, A. T., Adams, P. D., Clore, G. M., DeLano, W. L., Gros, P., Grosse-Kunstleve, R. W., Jiang, J. S., Kuszewski, J., Nilges, M., Pannu, N. S., Read, R. J., Rice, L. M., Simonson, T., and Warren, G. L. (1998) *Acta Crystallogr. Sect. D Biol. Crystallogr.* **54,** 905–921
29. Pedersen, K., Christensen, S. K., and Gerdes, K. (2002) *Mol. Microbiol.* **45,** 501–510
30. Wishart, D. S., and Sykes, B. D. (1994) *J. Biomol. NMR* **4,** 171–180
31. Orengo, C. A., and Thornton, J. M. (1993) *Structure* (*Lond.*) **1,** 105–120
32. Takagi, H., Kakuta, Y., Okada, T., Yao, M., Tanaka, I., and Kimura, M. (2005) *Nat. Struct. Mol. Biol.* **12,** 327–331
33. Gerdes, K., Moller-Jensen, J., and Bugge Jensen, R. (2000) *Mol. Microbiol.* **37,** 455–466
34. Holm, L., and Park, J. (2000) *Bioinformatics* (*Oxf.*) **16,** 566–567
35. Yajima, S., Inoue, S., Ogawa, T., Nonaka, T., Ohsawa, K., and Masaki, H. (2006) *Nucleic Acids Res.* **34,** 6074–6082
36. Sevcik, J., Lamzin, V. S., Dauter, Z., and Wilson, K. S. (2002) *Acta Crystallogr. Sect. D Biol. Crystallogr.* **58,** 1307–1313